Indian Journal of Pure & Applied Physics
Vol. 62, January 2024, pp. 23-28
DOI: 10.56042/ijpap.v62i1.5445

CO Gas Sensing Properties of Chemically Deposited ZnO: Al Thin Films

Th Ratanjit Singh[a], L Raghumani Singh[b*] & A Nabachandra Singh[c]

[a]Department of Physics, D.M. University, Imphal, Manipur 795 001, India

[b]Department of Physics, D.M. College of Science, D.M. University, Imphal, Manipur 795 001, India

[c]D.M. College of Commerce, D.M. University, Imphal, Manipur 795 001, India

Received 8 September 2023; accepted 28 November 2023

In this research work, the structural and optical properties of undoped and Al doped ZnO thin films are being reported. The nanocrystalline ZnO thin films were deposited on glass substrate by chemical bath deposition technique using zinc acetate (AR), triethanolamine (AR), sodium hydroxide (AR) as the source materials and aluminum nitrate as source of the dopant. The structural characterization was done by XRD (X-ray diffraction). The crystallite size was found to decrease on doping of Al. SEM (Scanning Electron Microscope) was employed to examine the surface morphology of thin films and formation of ZnO nanorod was observed. The optical band gap of thin films was studied by UV-Visible spectroscopy. The band gap energy was found to vary from 3.84 eV to 4.0 eV. The electrical and CO gas sensing properties of thin films were also investigated. For application purpose, the quick response of chemically synthesized ZnO thin films to CO gas was observed and the fast recovery in absence of CO gas was also observed.

Keywords: Chemical Bath Deposition; EDAX; Optical band gap; SEM; UV-Visible spectroscopy; XRD; Zinc Oxide

1 Introduction

ZnO is a semiconductor of wide-bandgap in the range from 3.10 eV to 3.37 eV[1] that belongs to group II-VII semiconductors. It is an n-type semiconductor that shows a crystal structure of hexagonal (wurtzite) type which is suitable for the fabrication of highly oriented thin films[2,3].

As compared to other gas sensor, the gas sensor based on metal oxide semiconductors is one of the most promising[4] candidate due to its high sensitivity and chemical stability[5]. Metal Oxide semiconductors such as SnO_2, ZnO, WO_2, TiO_2 are normally used as gas sensor[6,7]. Among the various applications, ZnO has shown to be helpful material for monitoring various pollutants gases like CO, SO_2, NO_2, NH_3 *etc*. because of its high sensitivity, good stability and controllable morphology[8,9].

Various reports show that the changes in particle morphology alter the electrical characteristics and reactivity of ZnO when interacting with gaseous species[10]. Experimental studies also shows that the sensitivity and selectivity of a metal-oxide gas sensors depends on the link between morphology, surface reactivity, and electrical properties. The enhancement in gas response with decrease in particle size is well studied[11–13]. The effect of dopant on grain size and gas sensor behavior has been extensively studied[14,15]. It is known that when the particle size is comparable to surface depletion layer, the energy band bending no longer depends on the surface but extends into the bulk of the grains and the response of gas sensor is dramatically enhanced.Various techniques *i.e*. vapor-phase transport, Pulse Laser Deposition, Chemical vapor deposition, electrochemical deposition, and Chemical bath deposition have been widely reported for the fabrication of ZnO[16]. All the methods except Chemical Bath Deposition method require highly sophisticated equipment, complex process, and high temperature. On the contrary Chemical Bath Deposition method does not require highly sophisticated equipment and can be operated easily at low temperatures and low cost. Further, it can provide different morphologies in ZnO nanostructure. So, in the present study, ZnO thin films were prepared by Chemical Bath Deposition method to investigate its sensing properties to CO gas.

2 Experimental Details

Prior to synthesis work, the substrates to be used for the deposition of ZnO thin films were cleaned ultrasonically in order to remove the surface impurity. For the fabrication of undoped ZnO thin film of 0.1 M, triethanolamine of 2M was added to Zinc

*Corresponding author: (E-mail: laishramraghumani204@gmail.com)

acetate dehydrate ($Zn(CH_3COO)_2.2H_2O$) solution of 0.1 M. Sodium hydroxide solution was added to precursor solution drop wise to maintain the pH value at 11. The cleaned glass substrate was immersed vertically at the center of the beaker maintaining temperature at 50 ℃ with continuous stirring at 150 rpm for 2 hrs and ZnO thin films are deposited on glass substrate. The films were washed with distilled water and dried at room temperature. The same procedure was followed for fabrication of Al-doped ZnO thin films of 0.1M using 1 % of $Al(NO_3)_3$.

2.2 Reaction Mechanism

$$Zn(CH_3COO)_2 2H_2O + TEA \rightarrow [Zn(TEA)]^{2+} + 2CH_3COO^-$$

$$[Zn(TEA)]^{2+} \rightarrow Zn^{2+} + TEA$$

$$2NaOH \rightarrow 2Na^+ + 2OH^-$$

$$Zn + 2OH^- \rightarrow Zn(OH)_2$$

$$Zn(OH)_2 \rightarrow ZnO + H_2O$$

$$Al(NO_3)_3 \rightarrow Al^{3+} + 3NO_3^-$$

$$Zn(OH)_2 + Al^{3+} \rightarrow ZnAlO + H_2O$$

3 Results and Discussion

3.1 Structural Characterization

The XRD patterns of undoped and Al doped ZnO thin films recorded in the range of 30° to 80° are shown in Fig. 1. The diffraction patterns of undoped and Al doped ZnO samples are indexed to hexagonal wurtzite crystal structure of ZnO as confirmed by JCPDS 96-152-9591. As seen in Fig. 1, the undoped ZnO thin film has a high preferential orientation along the (100) plane. Other diffraction peaks with weak intensity are also observed. However, the atomic density is very low for these peaks. Hence, (100) plane may be considered as the dominant plane for analysis. This result indicates that the film has a polycrystalline hexagonal wurtzite structure with

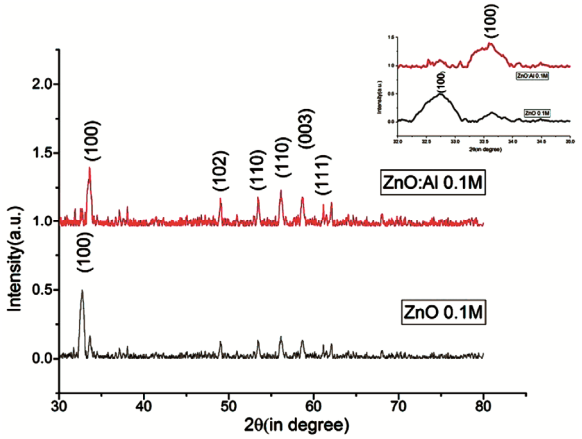

Fig. 1 — XRD Pattern of undoped and Al doped ZnO of 0.1M molarity.

a-axis orientation. Further, it has been observed that the peak intensity decreases with Al doping and width has become broader and FWHM (β) increases which results inthe formation of small crystallite. The broadening of peak width might be due to formation of imperfect crystal lattice with Al doping. H. Kim et.al(2000) have also found that with Al content the peak width becomes broader which proves that the crystallite size decreases with increasing the aluminium content in the targets[17]. Other similar result is also shown by Sahay and Nath[18] and Chen *et al.*[19] that the crystallite size decreases with increasing Al-doping. The replacement of Zn^{2+} by Al^{3+} produces a slight shift of diffraction peak (100) towards larger angle because of smaller radius of Al^{3+} (0.0535 nm) as compared to that of Zn^{2+} (0.0740 nm).This leads to conclusion that preferential orientation is attributable to internal strain of the film. The formation of other phases related to other impurities is not observed in the XRD pattern of ZnO:Al thin films. The crystallite size and lattice parameters of the prepared thin films of 0.1 M are calculated for the dominant peak corresponding to crystal plane (100) in the XRD pattern. The crystallite size is calculated by using Scherrer's formula

$$D = \frac{k\lambda}{\beta \cos\theta} \quad \ldots(1)$$

Where, λ = 1.5406 Å, k = 0.94,θ = Diffraction angle in degrees, β = FWHM in radian.

The d-spacing is calculated by Bragg's law,

$$n\lambda = 2dsin\theta \quad \ldots(2)$$

The lattice parameters are calculated by using the formula

$$\frac{1}{d^2} = \frac{4}{3}\left(\frac{h^2+hk+k^2}{a^2}\right) + \frac{l^2}{c^2} \quad \ldots(3)$$

Where, d = d- spacing; a, c are lattice constant and h,k,l are miller indices. The dislocation density is calculated by using the formula

$$\rho = \frac{1}{D^2} \quad \ldots(4)$$

Where, D = Crystallite size. The strain was calculated by using the tangent formula

$$\gamma = \frac{\beta}{4tan\theta} \quad \ldots(5)$$

where, β = FWHM in radian, θ = Diffraction angle in degrees.

The structural parameters of undoped and Al doped ZnO thin films of 0.1M are shown in Table 1. It is

Table 1 — Structural parameters of thin films estimated from XRD pattern.

Molarity	Crystal plane	Sample	Crystallite size D (nm)	d-spacing (Å)	Lattice constant, a (Å)	Dislocation Density, ρ (nm^{-2})	Strain (γ)
0.1M	(100)	ZnO	18.62	2.736412	3.24920	0.002882134	0.000595
		Al:ZnO	11.41	2.813809	3.35015	0.007678502	0.054698

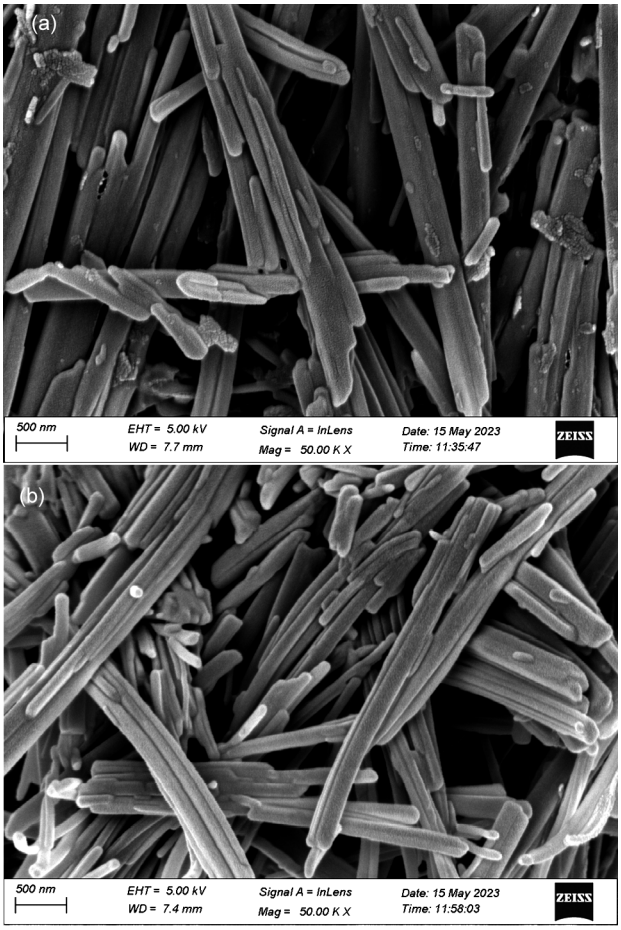

Fig. 2 — SEM images of (a) undoped ZnO of 0.1M. (b) ZnO:Al of 0.1M.

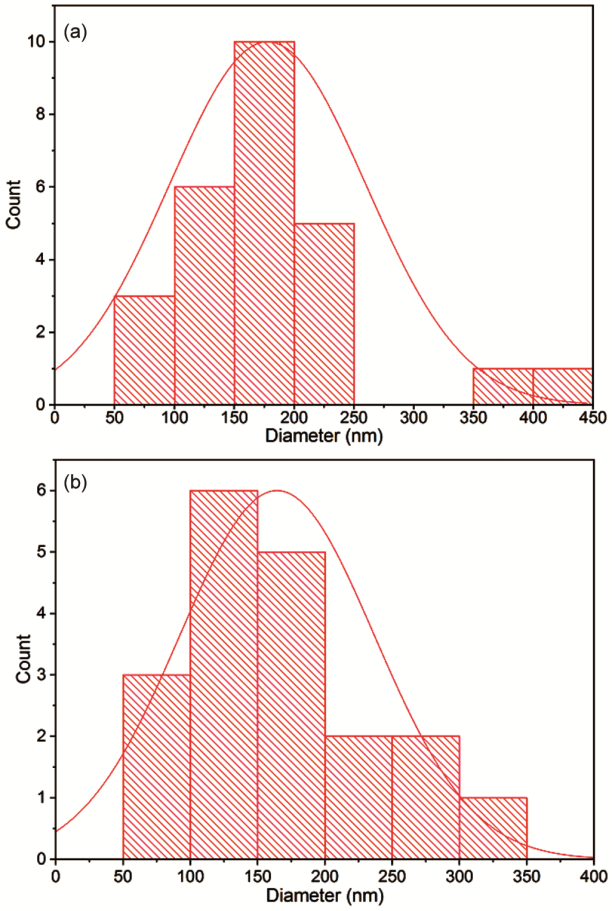

Fig. 3 — Histograms of (a) undoped ZnO 0.1M. (b) ZnO:Al of 0.1M.

found that the crystallite size decreases on doping of Albut the d-spacing, lattice parameter (a), dislocation density and strain of Al doped ZnO increase as compared to undoped ZnO.

3.2 Morphological Study

Figure 2 represents the SEM images of undoped and Al doped ZnO thin films of 0.1 M deposited on a glass substrate and it reveals the formation of ZnO nanorods. Further, it is also observed that the compactness of ZnO nanorods increases with Al doping. Fig. 3 represents the histogram *i.e.* frequency of occurrence versus diameter of the nanorods. The diameter of the nanorods is measured by using the Image J software and the data so obtained is used for plotting Histogram. From the histogram, the average diameter of the nanorods is found to be 177.89 nm for undoped ZnO and 164.43nm for Al doped ZnO thin films of 0.1M. It has been observed that the diameter of the ZnO nanorods decreases with Al doping as compared with undoped ZnO which is consistent with XRD results.

3.3 Optical Properties

The UV absorption spectra for the prepared thin films are shown in Fig. 4. The direct band gap energy of the prepared thin films can be estimated from the Tauc plot *i.e.* graph of hν versus $(\alpha h\nu)^2$ through the absorption coefficient α which is related with the band gap energy, E_g as:

$(\alpha h\nu)^2 = k(h\nu - E_g)$, where hν= Energy of incident light, K = constant.

The thickness of thin films is calculated by mass difference method (gravimetric method) using the

highly sensitive electronic balance and the thickness of the prepared film is calculated by using the formula, $t = \frac{m}{d \times A}$ where, m= mass, d= density and A= area of the prepared film. The thickness of the pure ZnO and ZnO:Al is found to be 162.53µm and 22.88µm respectively. The extrapolation of the straight line to $(\alpha h\nu)^2 = 0$ gives the value of band gap energy. From Fig. 5, the values of band gap energy of undoped and Al doped ZnO of 0.1M are found to be 3.84 eV and 4.0 eV respectively. It indicates that there is an increase in band gap energy of the prepared ZnO as compared to that of the bulk state (3.10 eV to 3.37 eV). The increase in band gap might be due to the quantum confinement effect. The decrease in particle size results in increase in surface volume ratio. The surface atom has lower coordination number and atomic interaction which increases the highest valence band energy and decreases the lowest unoccupied conduction band energy. This leads to increase in band gap[20]. It is also observed that with Al doping, there is an increase in band gap as compared to undoped ZnO. This broadening in band gap energy might be due to Moss-Burstein shift[21,22]. According to the Moss-Burstein theory, in a heavily doped Zinc oxide films, the donor electrons occupy states at the bottom of the conduction band. Since the Pauli principle prevents states from being doubly occupied and optical transitions are vertical, the valence electrons require an additional energy to be excited to higher energy states in the conduction band[23]. Hence, there is an increase in band gap energy with Al doping on ZnO.

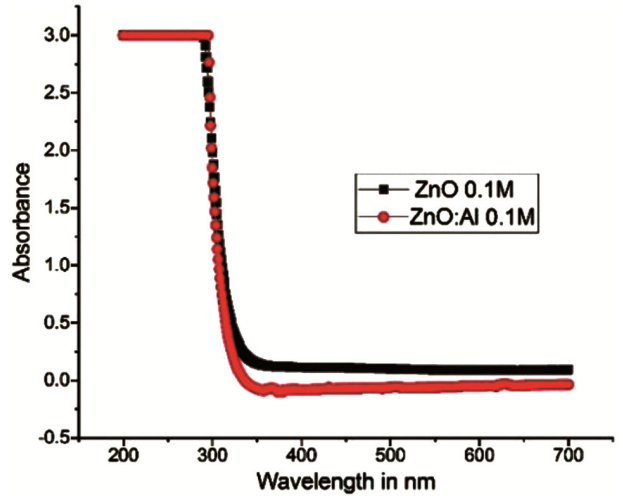

Fig. 4 — Absorbance spectra of ZnO and ZnO:Al thin films.

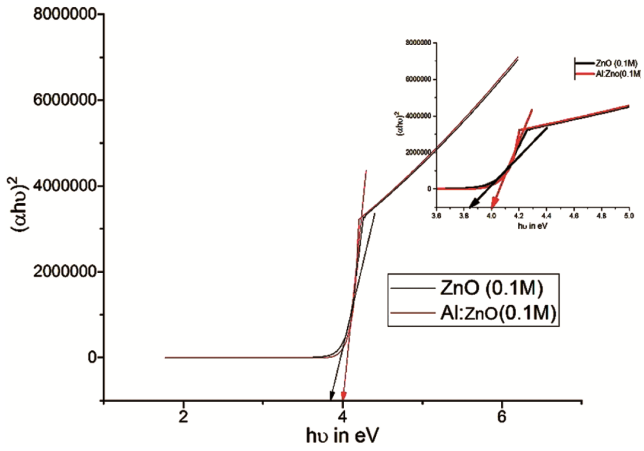

Fig. 5 — Tauc Plot of hν versus $(\alpha h\nu)^2$ of ZnO and ZnO:Al thin films.

3.4 I-V Characteristics

The I-V characteristics of forward bias for both undoped and Al doped ZnO of 0.1M are shown in Fig. 6. The current is measured by using a Digital Picoammeter (Model DPM-111) and a Digital regulated power supply (AEC VPS-300) is used as a power supply. From Fig. 6, it has been observed that the graphs show a non-linear rectification behaviour which confirms the formation of Schottky contact between ZnO and Copper contact. From the graphs, it has also been observed that the electrical resistance of the prepared ZnO thin films decreases with Al doping. The electrical resistance of pure ZnO is found to be 23.80 MΩ while that of ZnO:Al is 1.34 MΩ. Although there is an increase in band gap with Al doping, there is an increase in the conductivity of the ZnO:Al thin films. This might be due to the presence of extra free electrons with Aluminium doping.

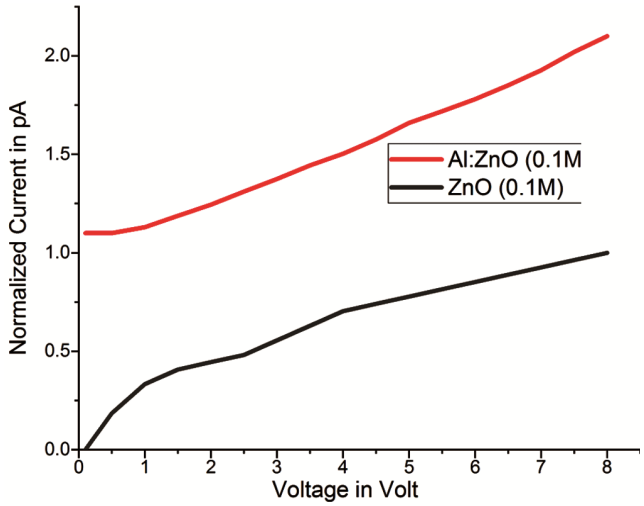

Fig. 6 — I-V characteristics of ZnO and ZnO:Al of 0.1M.

4 Gas sensing application of ZnO thin films

4.1 Sensing properties

The sensitivity of the gas S is defined by using the formula

$$S = \frac{R_a - R_g}{R_a}$$

Where, R_a and R_g are the resistance of the samples in presence of air and gas. When the prepared thin film sensor sample is kept under the exposure of CO air, the electrons are liberated by the oxygen ions into the conduction band and Carbon dioxide is formed and there is an increase in electron concentration which reduces the electrical resistance of the prepared thin film sensor.

Figure 7 shows the Schematic circuit diagram for testing CO gas sensor. From Fig. 8, it has been observed that the sensitivity of the CO gas increases with Al doping. This might be due to incorporation of Al with ZnO which leads to increase in stacking fault leading to an improvement of the gas sensing performance. The substitution of Al^{3+} ions instead of Zn^{2+}ions in the ZnO lattice leads to an increase in the gas response to CO and changes in the defect of ZnO. As the ionic radius of Al^{3+} is smaller than Zn^{2+}ions, the Al^{3+} ions can easily substitute the Zn^{2+} ions but it is necessary to maintain the electrical neutrality by compensating the valence charge of Zn site by releasing the electrons[24]. Hence there is a decrease in resistance of the prepared sensor thin film with Aluminium doping on ZnO. Thus, there is an increase in sensor performance with Aluminium doping.

4.2 Response and recovery time

The time required for the ZnO sensor to attain 90% of the maximum increase in conductance on exposure of the target gas is known as response time. The time required by the sensor to get back 10% of the maximum conductance when the flow of gas is switched off is known as recovery time. Fig. 8 shows response and recovery time of ZnO and ZnO:Al thin films of 0.1 M.. From Fig. 8, it is observed that the response was very quick (~ 9 s for ZnO and ~ 7 s for ZnO:Al) while the recovery was fast (~50 s for ZnO and ~45 s for ZnO:Al) to CO gas at 100 ppm concentration. Fast response may be due the reducing nature of CO gas.

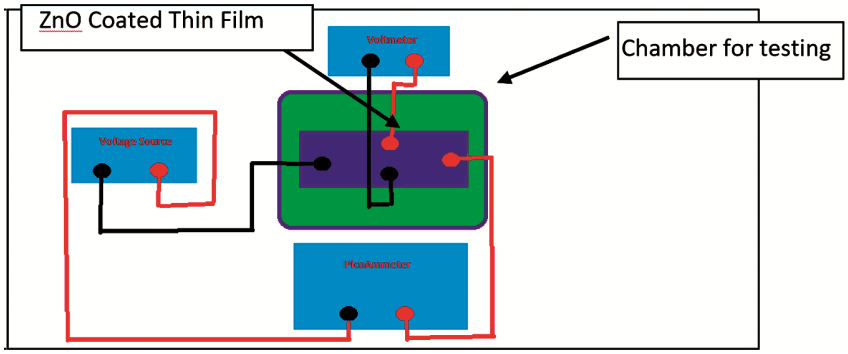

Fig. 7 — Schematic circuit diagram for testing CO gas sensor.

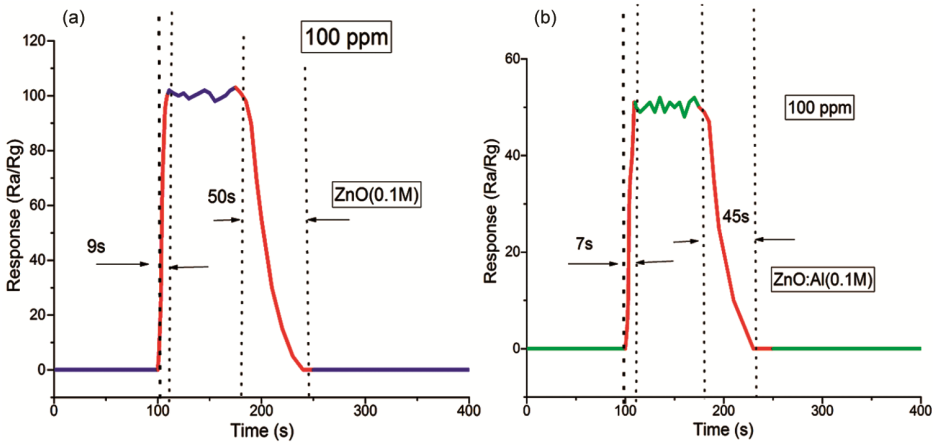

Fig. 8 — Response and recovery of (a) ZnO of 0.1 M and (b) ZnO:Al of 0.1 M at room temperature with a fixed biased voltage of 5V.

5 Conclusion

Pure (undoped) and Al doped ZnO thin films were successfully deposited on glass substrate by Chemical Bath Deposition method at 50 °C. The structural characterization confirmed that both pure and Al doped ZnO films possess wurtzite hexagonal structure. It was also observed that the crystallite size decreases on doping of Aluminium *i.e* from 18.62 nm (for ZnO) to 11.41 nm (for ZnO:Al). The pure and Al doped ZnO thin films exhibit rod shaped morphologies. The diameter of ZnO nanorod as estimated from histogram was found to be 177.89 nm for ZnO and 164.43 nm for ZnO:Al respectively. The band gap energy of thin films increases with doping of Al on ZnO *i.e*. from 3.84 eV to 4.0 eV. This in turn increase the sensitivity of ZnO thin film to CO gas. The response time of ZnO:Al to CO gas *i.e*. ~ 7 s is smaller than that of ZnO to CO gas *i.e*. ~ 9 s. Hence, ZnO:Al thin film can work as the excellent and more suitable gas sensor for detecting poisonous CO gas which is harmful to human beings.

Acknowledgment

The authors are thankful to Nanoelectronics Research Laboratory, Department of Electronics, D.M. College of Science, Imphal for synthesis of sample, I-V and CO gas sensing measurement, Physics Department, Manipur University for XRD measurement, Sophisticated Analytical Instrumentation Centre (SAIC), Institute of Advanced Study in Science and Technology (IASST), Guwahati (under the Department of Science & Technology, Government of India) for SEM analysis, Chemistry Department, Dhanamanjuri University for UV measurement.

Reference

1 Davis K , Yarbrough R , Froeschle M, White J & Rathnayake H B, *RSC Adv*, 26 (2019).
2 Gutierrez F M, Olive P L, Banuelos A, Orrantia E, Nino N, Sanchez E M, Ruiz F, Bach H & Gay Y A, *Nanomed Nanotechnol Biol Med*, 6 (2010) 681.
3 Tamaki N, Onodera A, Sawada T & Yamashita H, *J Korean Phys Soc*, 29 (1996) S668.
4 Yuliarto B, Gumilar G, Zulhendri D W, Nugraha & Septiani N L W, *Acta Physisca Polonica A*, 1313 (2017).
5 Septiani N L W, *Nano Composites Multiwalled Carbon Nanotubes-Zinc Oxide (MWCNTZnO) as Toluene Gas Sensor,* Thesis (Bandung: Institute Technology Bandung) (2015).
6 Yuliarto B, Julia S, Septiani N LW, Iqbal M, Ramadhani M F & Nugraha, *J Eng Technol Sci*, 47 (2015) 76.
7 Yuliarto B, Ramadhani M F, Wieno H & Nugraha, *Int J Mater Sci Eng*, 2 (2014) 15.
8 Rezabeigy S, Behboudnia M & Nobari N, *Proc Mater Sci*, 11 (2015) 364.
9 Jabeen M, Iqbal M A, Kumar R V, Ahmed M & Javed M T, *Chin Phys Soc*, 23 (2014) 018504.
10 Tian S, Yang F, Zeng D & Xie C, *J Phys Chem C*, 116 (2012) 10586.
11 Xu C, Tamaki J, Miura N & Yamazoe N, *Sens Actuators B*, 3 (1991) 147.
12 Ansari Z A, Ansari S G, Ko T & Oh J H, *Sens Actuators B*, 87 (2002) 105.
13 Rothschild A & Komem Y, *J Appl Phys*, 95 (2004) 6374.
14 Sun T, Donthu S, Sprung M, Aquila K D, Jiang Z, Srivastava A, Wang J & Dravid V P, *Acta Mater*, 57 (2009) 1095.
15 Zhang G & Liu M, *Sens Actuators B*, 69 (2000) 144.
16 Tian Z R, Voigt J A, Liu J, McKenzie B, McDermott M J, Rodriguez M A, Konishi H & Xu H, *Nature Mater*, 2 (2003) 821.
17 Kim H, Pique A, Horwitz J S, Murata H, Kafafi Z H, Gilmore C M & Chrisey D B, *Thin Solid Films*, 377 (2000) 798.
18 Sahay P P & Nath R K, *Sens Actuators B-Chem*, 134 (2008) 654.
19 Chen J, Chen D, He J, Zhang S & Chen Z, *Appl Surf Sci*, 255 (2009) 9413.
20 Chand P, Gaur A & Kumar A, *J Alloys Compd*, 539 (2012) 174.
21 Sernelius B E, Berggren K F, Jim Z C, Hamberg I & Granqvist C G, *Phys Rev B*, 37 (1988) 10244.
22 Shan F K & Yu Y S, *J Eur Ceram Soc*, 24 (2004) 1869.
23 Lee K E, Wang M, Kim E J & Hahn S H, *Curr Appl Phys*, 9 (2009) 683.
24 Kumar M, Singh B, Yadav P, Bhatt V, Kumar M, Singh K, Abhyankar A C, Kumar A & Yun J-H, *Ceram Int*, 43 (2016).